# Supplementary Materials for "Quantum nonlinear magnonics: Magnon squeezing in the quantum regime"

Yuan-Chao Weng,[1] Da Xu,[1] Zhen Chen,[2] Li-Zhou Tan,[1] Xu-Ke Gu,[1] Jie Li,[1] Hai-Feng Yu,[2] Shi-Yao Zhu,[1,3] Xuedong Hu,[4] Franco Nori,[5,6] and J. Q. You[1,3]

[1] *Zhejiang Province Key Laboratory of Quantum Technology and Device, School of Physics, and State Key Laboratory for Extreme Photonics and Instrumentation, Zhejiang University, Hangzhou 310027, China*
[2] *Beijing Key Laboratory of Fault-Tolerant Quantum Computing, Beijing Academy of Quantum Information Sciences, Beijing 100193, China*
[3] *College of Optical Science and Engineering, Zhejiang University, Hangzhou 310027, China*
[4] *Department of Physics, University at Buffalo, SUNY, Buffalo, NY, 14260-1500, USA*
[5] *Quantum Computing Center, RIKEN, Wakoshi, Saitama 351-0198, Japan*
[6] *Department of Physics, University of Michigan, Ann Arbor, Michigan 48109-1040, USA*

## CONTENTS



## I. DEVICE PARAMETERS

The device consists of a 1 mm-diameter yttrium iron garnet (YIG) sphere and a superconducting qubit placed near the magnetic- and electric-field antinode of a rectangular three-dimensional (3D) microwave cavity, respectively. The whole device is anchored to the base plate of a dilution refrigerator at $\sim 10$ mK. Compared to our previous implementations [1, 2], several optimizations are made to enhance system's cooperativity to

$$C = \frac{4g_{qm}^2}{\gamma_q \gamma_m} \approx 1.0 \times 10^4, \tag{S1}$$

i.e., an order-of-magnitude enhancement over the previous implementations. These optimizations include:

1. Reduced cavity dimensions, which increase the mode density. The cavity size is decreased from $62 \times 36 \times 2.5$ mm$^3$ to $58 \times 41 \times 2$ mm$^3$, thereby enhancing the coupling strength, $g_{qc}$ ($g_{qm}$), between the qubit (magnon) and the considered cavity mode $\mathrm{TE}_{102}$.

2. An optimized frequency configuration for the qubit, magnon and $\mathrm{TE}_{102}$ mode. The frequency detuning between the $\mathrm{TE}_{102}$ mode and qubit (magnon) is reduced, leading to a significant increase of the qubit-magnon coupling strength $g_{qm}$.

3. Enhanced coherence of the Kittel mode by using a YIG sphere made of high-quality material and with reduced surface roughness.

The device parameters are detailed in Table. S1.

TABLE S1. **Device parameters**

| Parameter | Value |
|---|---|
| $\omega_{ge}/2\pi$ (idle) | 6.107 GHz |
| $\omega_{ef}/2\pi$ (idle) | 5.858 GHz |
| $\eta/2\pi$ (anharmonicity) | −0.249 GHz |
| $T_{1,q}$ | 1.10 $\mu$s |
| $T_\phi$ | 1.45 $\mu$s |
| $\gamma_q/2\pi$ | 0.14 MHz |
| $\omega_m/2\pi$(idle) | 6.231 GHz |
| $\gamma_m/2\pi$ | 1.10 MHz |
| $\omega_{\mathrm{TE101}}/2\pi$ | 4.512 GHz |
| $\omega_{\mathrm{TE102}}/2\pi$ | 6.364 GHz |
| $\omega_{\mathrm{TE103}}/2\pi$ | 8.572 GHz |
| $\kappa_{\mathrm{TE101}}/2\pi$[a] | 0.36 MHz |
| $\kappa_{\mathrm{TE102}}/2\pi$ | 0.73 MHz |
| $\kappa_{\mathrm{TE103}}/2\pi$ | 0.76 MHz |
| $g_{qc}/2\pi$ | 86MHz |
| $g_{mc}/2\pi$ | 57MHz |

[a] $\kappa$ stands for the total linewidth of the cavity mode.

## II. EFFECTIVE HAMILTONIAN

As in the previous implementations [1, 2], we utilize the Autler-Townes (AT) effect [3] to achieve frequency tunability for the qubit (see Fig. S3). We consider the ground, first-excited, and second-excited states of the transmon, denoted as $|g\rangle$, $|e\rangle$ and $|f\rangle$, respectively. A strong microwave drive resonant with the $|e\rangle \rightarrow |f\rangle$ transition ($\omega_{\mathrm{AT}} = \omega_{ef}$) is applied to the transmon, hybridizing the states $|e\rangle$ and $|f\rangle$ into dressed states $|+\rangle$ and $|-\rangle$, with $|\pm\rangle = \frac{1}{\sqrt{2}}(|e\rangle \pm |f\rangle)$. The frequencies of these dressed states vary linearly with the drive strength $\Omega_{\mathrm{AT}}$, i.e., $\omega_\pm = \omega_{ge} \pm \frac{\Omega_{\mathrm{AT}}}{2}$. Here, we choose $|g\rangle$ and $|+\rangle$ as the two basis states of the tunable qubit.

In our experimental setup, the cavity mode $\mathrm{TE}_{102}$ is far-detuned from both the magnon and the qubit, so the qubit and the magnon can be effectively coupled via exchanging virtual cavity photons [4], and the system Hamiltonian is reduced to [1, 2]

$$H/\hbar = \frac{1}{2}\omega_q\sigma_z + \omega_m a^\dagger a + g_{qm}(\sigma_+ a + \sigma_- a^\dagger), \tag{S2}$$

where $\omega_q$ is the transition frequency of the tunable qubit, $\omega_m$ is the frequency of the magnon, $\sigma_+ = |+\rangle\langle g|$, $\sigma_- = |g\rangle\langle +|$, $a$ ($a^\dagger$) is the magnon annihilation (creation) operator, and $g_{qm}$ is the effective coupling strength between the tunable qubit and the magnon.

By applying a unitary transformation [5] $U = \exp[\Lambda(a^\dagger\sigma_- - a\sigma_+)]$, with

$$\Lambda = \frac{\arctan\left(\frac{2g_{qm}}{\Delta_{qm}}\sqrt{a^\dagger a + |+\rangle\langle +|}\right)}{2\sqrt{a^\dagger a + |+\rangle\langle +|}}, \tag{S3}$$

the Hamiltonian can be exactly diagonalized to

$$H_{\mathrm{diag}}/\hbar = UHU^\dagger/\hbar = \omega_m a^\dagger a + \frac{1}{2}\omega_q\sigma_z - \frac{\Delta_{qm}}{2}\left[1 - \sqrt{1 + 4\frac{g_{qm}^2}{\Delta_{qm}^2}(a^\dagger a + |+\rangle\langle +|)}\right]\sigma_z. \tag{S4}$$

In the experiment, the qubit and magnon are tuned in the dispersive regime, i.e., $|g_{qm}/\Delta_{qm}| \ll 1$. Thus, we can keep the leading terms in the Hamiltonian by expanding $H_{\mathrm{diag}}$ to the third order in $g_{qm}/\Delta_{qm}$:

$$H'/\hbar \approx (\omega_m - \delta)a^\dagger a - \delta(a^\dagger a)^2\sigma_z + \left[\omega_q + 2\chi(a^\dagger a + \frac{1}{2})\right]\frac{\sigma_z}{2}, \tag{S5}$$

where $\chi = g_{qm}^2/\Delta_{qm} - g_{qm}^4/\Delta_{qm}^3$ is the dispersive shift and $\delta = g_{qm}^4/\Delta_{qm}^3$ is the magnon self-Kerr coefficient. Given a relatively large detuning between the magnon and qubit, the qubit is expected to remain predominantly in the ground state $|g\rangle$ when we drive the magnon system to enable Kerr evolution. This is confirmed by our experimental data, because the probability of the qubit being in $|g\rangle$ is measured to be $P_g > 0.94$ during the Kerr evolution of the magnon. Therefore, $H'$ can be safely projected onto the $\sigma_z = -1$ manifold (with the qubit in the ground state), yielding an effective Hamiltonian for the magnon,

$$H_{\text{eff}}/\hbar = (\omega_m - \chi - \delta)a^\dagger a + \delta(a^\dagger a)^2, \tag{S6}$$

which is Eq. (3) in the main text of the manuscript. From the experimental measurements, we have $g_{qm}/2\pi = 20$ MHz and $\Delta_{qm}/2\pi = 76$ MHz, giving rise to $\delta/2\pi = 0.36$ MHz. As shown in our experiment, this self-Kerr coefficient is sufficiently large to observe magnon squeezing in the quantum regime.

## III. MAGNON-ASSISTED RAMAN PROCESS

The Wigner function of a magnon state $\rho_m$ is extracted by measuring the parity of the displaced magnon state. Specifically, the Wigner function $W(\alpha)$ is given by $W(\alpha) = (2/\pi)\langle P\rangle$, where $\langle P\rangle \equiv (2/\pi)\text{Tr}[D(-\alpha)\rho_m D(\alpha)P]$, with $D(\alpha) = \exp(\alpha a^\dagger - \alpha^* a)$ being the magnonic displacement operator and $P = \exp(i\pi a^\dagger a)$ the magnonic parity operator. The expectation value of the parity operator is $\langle P\rangle = (2/\pi)\sum_n (-1)^n \tilde{\rho}_{nn}(\alpha)$, where $\tilde{\rho}_{nn}(\alpha)$ denotes the density matrix element corresponding to the magnon population in the Fock state $|n\rangle$, where $n$ denotes the magnon number.

A resonant swap between the qubit and magnon is essential for the magnon measurement. However, in our system the frequency detuning between the qubit transition $|g\rangle \to |e\rangle$ and the Kittel mode, $\Delta_{ge,m}/2\pi = (\omega_m - \omega_{ge})/2\pi = 124$ MHz, is comparable to the qubit anharmonicity $\eta/2\pi = (\omega_{ef} - \omega_{ge})/2\pi = -249$ MHz. This necessitates a strong AT drive, with a Rabi frequency of the same order as the qubit anharmonicity, to bring the qubit into resonance with the magnon mode. Conversely, the strong AT drive can cause the qubit to have a non-negligible state leakage, because the drive can undesirably excite the qubit from $|g\rangle$ to $|e\rangle$ as well.

To address this challenge, we implement a magnon-assisted Raman process to facilitate the qubit-magnon swap. The key of this method involves applying a suitable drive to the qubit; when the drive frequency matches the detuning between the $|g\rangle \to |f\rangle$ transition frequency and the magnon frequency (i.e., $\omega_d \approx \omega_{ge} + \omega_{ef} - \omega_m$), it mediates the coupling between the states $|g, n+1\rangle$ and $|f, n\rangle$. This technique was previously utilized to deterministically prepare the quantum states of cavity photons [6].

Under the microwave drive with frequency $\omega_d$ and amplitude $\Omega$, the total Hamiltonian of the magnon-transmon system is given by [6, 7]

$$H_{\text{tot}}/\hbar = \omega_m a^\dagger a + \omega_{ge} b^\dagger b + \frac{\eta}{2} b^\dagger b^\dagger b b + g(ab^\dagger + a^\dagger b) + \frac{\Omega}{2}(b + b^\dagger)(e^{i\omega_d t} + e^{-i\omega_d t}), \tag{S7}$$

where $g$ is the coupling strength between the magnon and transmon, and $a$ ($a^\dagger$) is the magnon annihilation (creation) operator. The transmon is treated as a nonlinear oscillator, with its annihilation operator $b$ given by [6, 7] $b \equiv |g\rangle\langle e| + \sqrt{2}|e\rangle\langle f| + \sqrt{3}|f\rangle\langle h| + \ldots$, where $|g\rangle, |e\rangle, |f\rangle, |h\rangle, \ldots$ denote the ground, first-excited, second-excited, third-excited state, etc. of the transmon, respectively. When truncating the energy levels of the transmon at the second-excited state, i.e., approximating it as a three-level system, we have

$$\begin{aligned} H_{\text{tot}}/\hbar = {} & \omega_m a^\dagger a + \omega_{ge}|e\rangle\langle e| + (2\omega_{ge} + \eta)|f\rangle\langle f| + g_{ge,m}(a|e\rangle\langle g| + a^\dagger|g\rangle\langle e|) + \sqrt{2}g_{ge,m}(a|f\rangle\langle e| + a^\dagger|e\rangle\langle f|) \\ & + \frac{\Omega}{2}(|e\rangle\langle g| + |g\rangle\langle e|)(e^{i\omega_d t} + e^{-i\omega_d t}) + \frac{\sqrt{2}\Omega}{2}(|f\rangle\langle e| + |e\rangle\langle f|)(e^{i\omega_d t} + e^{-i\omega_d t}), \end{aligned} \tag{S8}$$

where $g_{ge,m} \equiv g$ is the coupling strength between the transmon $|g\rangle \to |e\rangle$ transition and the magnon.

In the rotating frame with respect to the drive, a unitary transformation $R = \exp[i\omega_d t(a^\dagger a + |e\rangle\langle e| + 2|f\rangle\langle f|)]$ is applied to the system and the Hamiltonian is converted to

$$H_{\text{rot}} = RH_{\text{tot}}R^\dagger - i\hbar R\frac{\partial R^\dagger}{\partial t} \equiv H_{\text{JC}} + H_d, \tag{S9}$$

with

$$\begin{aligned} H_{\rm JC}/\hbar &= \omega_m^{\rm rot} a^\dagger a + \omega_{ge}^{\rm rot}|e\rangle\langle e| + (\omega_{ge}^{\rm rot}+\omega_{ef}^{\rm rot})|f\rangle\langle f| + g_{ge,m}(a|e\rangle\langle g| + a^\dagger|g\rangle\langle e|) + \sqrt{2}g_{ge,m}(a|f\rangle\langle e| + a^\dagger|e\rangle\langle f|), \\ H_d/\hbar &= \frac{\Omega}{2}(|e\rangle\langle g| + |g\rangle\langle e| + |e\rangle\langle g|e^{i(2\omega_d)t} + |g\rangle\langle e|e^{-i(2\omega_d)t}) + \frac{\sqrt{2}\Omega}{2}(|f\rangle\langle e| + |e\rangle\langle f| + |f\rangle\langle e|e^{i(2\omega_d)t} + |e\rangle\langle f|e^{-i(2\omega_d)t}) \\ &\approx \frac{\Omega}{2}(|e\rangle\langle g| + |g\rangle\langle e|) + \frac{\sqrt{2}\Omega}{2}(|f\rangle\langle e| + |e\rangle\langle f|), \end{aligned} \tag{S10}$$

where $\omega_m^{\rm rot} = \omega_m - \omega_d$, $\omega_{ge}^{\rm rot} = \omega_{ge} - \omega_d$, and $\omega_{ef}^{\rm rot} = \omega_{ef} - \omega_d$. In $H_d$, the fast oscillating terms are neglected under the rotating-wave approximation.

We now try to diagonalize the Hamiltonian. We start with the basis of the qubit-magnon product state $|q,n\rangle$, where $q = g, e, f$ represents the three qubit states, while $n$ is the number of magnons. Since $g_{ge,m}/2\pi \approx 28$ MHz is much smaller than the frequency detunings $(\omega_m^{\rm rot} - \omega_{ge}^{\rm rot})/2\pi = (\omega_m - \omega_{ge})/2\pi = 124$ MHz, and $(\omega_m^{\rm rot} - \omega_{ef}^{\rm rot})/2\pi = (\omega_m - \omega_{ef})/2\pi = (\omega_m - \omega_{ef} - \eta)/2\pi = 373$ MHz, we can treat the coupling term $g_{ge,m}(a|e\rangle\langle g| + a^\dagger|g\rangle\langle e|) + \sqrt{2}g_{ge,m}(a|f\rangle\langle e| + a^\dagger|e\rangle\langle f|)$ in $H_{\rm JC}$ as a perturbation and employ the perturbation theory to analytically derive the eigenstates and eigenenergies of $H_{\rm JC}$. Up to first order in $g_{ge,m}$, the eigenstates of $H_{\rm JC}$ are

$$\begin{aligned} |g,n\rangle_{\rm D} &= |g,n\rangle + \frac{g_{ge,m}\sqrt{n}}{\omega_m - \omega_{ge}}|e,n-1\rangle, \\ |e,n\rangle_{\rm D} &= |e,n\rangle + \frac{g_{ge,m}\sqrt{2n}}{\omega_m - \omega_{ef}}|f,n-1\rangle - \frac{g_{ge,m}\sqrt{n+1}}{\omega_m - \omega_{ge}}|g,n+1\rangle, \\ |f,n\rangle_{\rm D} &= |f,n\rangle - \frac{g_{ge,m}\sqrt{2(n+1)}}{\omega_m - \omega_{ef}}|e,n+1\rangle, \end{aligned} \tag{S11}$$

and the corresponding eigenenergies up to first order in $g_{ge,m}$ are

$$\begin{aligned} \varepsilon_{g,n}^{\rm D}/2\pi &= n(\omega_m - \omega_d), \\ \varepsilon_{e,n}^{\rm D}/2\pi &= n(\omega_m - \omega_d) + (\omega_{ge} - \omega_d), \\ \varepsilon_{f,n}^{\rm D}/2\pi &= n(\omega_m - \omega_d) + 2(\omega_{ge} - \omega_d) + \eta, \end{aligned} \tag{S12}$$

where the subscript (superscript) D denotes states (energies) in the eigenstate basis. In its eigenstate basis, the Hamiltonian $H_{\rm JC}$ is now diagonalized,

$$H_{\rm JC}^{\rm D}/\hbar = \sum_n (\varepsilon_{g,n}^{\rm D}|g,n\rangle_{\rm D}\langle g,n|_{\rm D} + \varepsilon_{e,n}^{\rm D}|e,n\rangle_{\rm D}\langle e,n|_{\rm D} + \varepsilon_{f,n}^{\rm D}|f,n\rangle_{\rm D}\langle f,n|_{\rm D}). \tag{S13}$$

The driving part of the Hamiltonain, $H_d$, can now be written in terms of the $H_{\rm JC}$ eigenstates. In particular, by setting the drive frequency at $\omega_d = 2\omega_{ge} + \eta - \omega_m$, $|g,n+1\rangle_{\rm D}$ and $|f,n\rangle_{\rm D}$ become resonant, i.e., $\varepsilon_{g,n+1}^{\rm D} = \varepsilon_{f,n}^{\rm D}$ (see Fig. S1 for the energy level diagram). These resonant states play a dominant role in the coupling induced by the microwave drive. $H_d$ can now be written as

$$\begin{aligned} H_d^{\rm D}/\hbar &= \sum_{im,jn} \langle i,m|_{\rm D}(H_d/\hbar)|j,n\rangle_{\rm D}|i,m\rangle_{\rm D}\langle j,n|_{\rm D}, \\ &\approx \sum_n \langle g,n+1|_{\rm D}(H_d/\hbar)|f,n\rangle_{\rm D}|g,n+1\rangle_{\rm D}\langle f,n|_{\rm D} + {\rm H.c.} \\ &= \sum_n g_{ge,m}\Omega\sqrt{\frac{n+1}{2}}\frac{\eta}{\Delta_{ge,m}(\eta - \Delta_{ge,m})}(|g,n+1\rangle_{\rm D}\langle f,n|_{\rm D} + |f,n\rangle_{\rm D}\langle g,n+1|_{\rm D}), \end{aligned} \tag{S14}$$

where $i,j = g,e,f$ denote the transmon states and $m,n = 0,1,2,...$ denote the magnon states. Equation (S14) indicates a Jaynes-Cummings coupling between the qubit and magnon. The microwave-induced coupling strength is hence given by

$$g_n = \langle g,n+1|_{\rm D}H_d|f,n\rangle_{\rm D} = g_{ge,m}\Omega\sqrt{\frac{n+1}{2}}\frac{\eta}{\Delta_{ge,m}(\eta - \Delta_{ge,m})} \equiv \sqrt{n+1}g_0. \tag{S15}$$

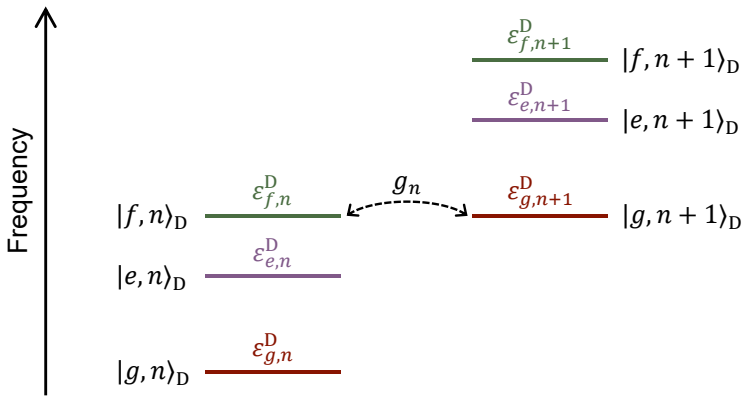


FIG. S1. **Energy level diagram of the qubit-magnon system in the rotating frame of the microwave drive.** The states $|f,n\rangle_{\mathrm{D}}$ and $|g,n+1\rangle_{\mathrm{D}}$ become resonant in the rotating frame of the drive at $\omega_d$ and the coupling strength $g_n$ between them is controlled by the amplitude $\Omega$ of the drive.

Equation (S15) demonstrates that the induced coupling strength between $|f,n\rangle_{\mathrm{D}}$ and $|g,n+1\rangle_{\mathrm{D}}$ is proportional to $\Omega$, a result confirmed by our experimental measurements (see Fig. 1c in the main text). Because the coupling strength $g_{ge,m}$ is much smaller than the frequency detunings $\omega_m-\omega_{ge}$ and $\omega_m-\omega_{ef}$, as a reasonable approximation, we can adopt $|g,n+1\rangle_{\mathrm{D}}\approx|g,n+1\rangle$ and $|f,n\rangle_{\mathrm{D}}\approx|f,n\rangle$ for an extremely low excitation of magnons (e.g., $|g,1\rangle_{\mathrm{D}}\approx|g,1\rangle$ and $|f,0\rangle_{\mathrm{D}}\approx|f,0\rangle$ for $n=0$), and $g_n\equiv\sqrt{n+1}g_0$ is approximately the coupling strength used for state swap between $|g,n+1\rangle$ and $|f,n\rangle$.

## IV. NUMERICAL SIMULATIONS AND DATA PROCESSING

### A. Numerical simulation of the Kerr evolution

We employ the Lindblad master equation to simulate the quantum-state evolution of the Kittel mode. In our experiment, we apply a microwave drive near resonance with the magnon frequency ($\omega_{m,d}\approx\omega_m$) to induce Kerr evolution in the magnon mode. In the rotating frame of the drive, the driven Kittel mode with Kerr nonlinearity is described by the Hamiltonian:

$$H^D_{\mathrm{Kerr}}/\hbar=\Delta_{m,d}a^\dagger a+\delta(a^\dagger a)^2+\frac{\Omega_{m,d}}{2}(a+a^\dagger). \tag{S16}$$

where $\Delta_{m,d}=\omega_{m,d}-\omega_m+\chi+\delta$ represents the drive detuning (in the experiment, we have $\Delta_{m,d}\approx0$) and $\Omega_{m,d}$ is the drive strength. The driven Kittel mode exhibits Kerr nonlinearity, characterized by the $(a^\dagger a)^2$ term, which modifies the dynamics of the magnons.

We simulate the magnon-state evolution via the Lindblad master equation based on $H^D_{\mathrm{Kerr}}$:

$$\frac{d\rho}{dt}=-\frac{i}{\hbar}[H^D_{\mathrm{Kerr}},\rho]+\frac{1}{2}[2L\rho L^\dagger-\rho L^\dagger L-L^\dagger L\rho], \tag{S17}$$

where $L=\sqrt{\gamma_m}a$ is the Liouville quantum jump operator for the magnon, with a linewidth $\gamma_m/2\pi=1.10$ MHz for the Kittel mode. By numerically solving Eq. (S17) using QuTip [8], we obtain the magnon density matrices at different evolution times. From these density matrices, we calculate the physical properties, such as the variances and mean number of magnons, as a function of time.

### B. Density-matrix construction

The density matrices of the squeezed magnon states are constructed using the maximum likelihood estimation (MLE) method. This process aims to find the most likely density matrix $\rho$ that corresponds to the measured Wigner function.

The Wigner function $W(\alpha)$ of a magnon state $\rho$ is related to the expectation value of the magnonic parity operator via $W(\alpha) = (2/\pi)P(\alpha)$, where $P(\alpha)$ denotes the parity of a displaced magnon state,

$$P(\alpha) = \mathrm{Tr}[D(-\alpha)\rho D(\alpha)P], \tag{S18}$$

where $D(\alpha) = e^{\alpha a^\dagger - \alpha^* a}$ is the magnonic displacement operator and $P = e^{i\pi a^\dagger a}$ is the magnonic parity operator. In the maximum likelihood estimation process, the density matrix elements $\rho_{ij}$ are treated as parameters. For the magnon Fock states, the maximum occupation number of magnons is truncated at $n_{\max} = 6$ in our numerical simulations.

Using Eq. (S18), we generate a hypothetical density matrix $\rho$ that yields a calculated parity $P^{(\mathrm{cal})}(\alpha)$, which can then be compared with the experimentally measured parity $P^{(\mathrm{exp})}(\alpha)$ for different values of $\alpha$. We minimize the cost function: $\sum_\alpha [P^{(\mathrm{cal})}(\alpha) - P^{(\mathrm{exp})}(\alpha)]^2$ numerically by considering all physically valid density matrices $\rho$, subject to the constraints that $\rho$ is Hermitian, normalized and positive semi-definite. The resulting density matrix is then our best estimate of the generated magnon state. In the main text, three constructed density matrices are presented in Fig. 2b, corresponding to the magnonic vacuum state and squeezed states generated at the evolution times $t = 0$, 100, and 200 ns, respectively.

### C. Variance of the general quadrature

To quantify the degree of squeezing for the magnon state, we calculate the variance of the general quadrature from the constructed density matrices. The general quadrature of the magnon mode is expressed as $\tilde{X}(\theta) = \cos(\theta)X + \sin(\theta)P$, where $X \equiv a + a^\dagger$ and $P \equiv -i(a - a^\dagger)$ represent the position and momentum quadratures of the magnon mode, respectively, and $\theta$ gives the angle of orientation in phase space. For the magnon state $\rho$, the variance of $\tilde{X}(\theta)$, denoted as $V(\tilde{X})$, is calculated via

$$V(\tilde{X}) = \langle \tilde{X}^2 \rangle - \langle \tilde{X} \rangle^2 = \mathrm{Tr}[\rho \tilde{X}^2] - (\mathrm{Tr}[\rho \tilde{X}])^2. \tag{S19}$$

By selecting a large number of $\theta$ values within the range from 0 to $2\pi$ and calculating the variance for each, the minimum value of $V(\tilde{X})$ (i.e., $V_{\min}$) can be obtained. However, this approach consumes a large computation resource because a substantial number of $\theta$ values must be chosen to accurately determine $V_{\min}$. For computational efficiency, we determine the minimum variance by calculating the minimum eigenvalue of the covariance matrix $C$:

$$V_{\min} = \min\{\mathrm{eig}[C]\}, \tag{S20}$$

where the covariance matrix $C$ is given by $C = \begin{bmatrix} c_{11} & c_{12} \\ c_{21} & c_{22} \end{bmatrix}$, with the elements $c_{ij}$ defined as

$$c_{ij} = \mathrm{Tr}[\rho(\tilde{X}_i \tilde{X}_j + \tilde{X}_j \tilde{X}_i)/2] - \mathrm{Tr}[\rho \tilde{X}_i]\mathrm{Tr}[\rho \tilde{X}_j], \quad i, j = 1, 2, \tag{S21}$$

where $\tilde{X}_1 = X$ and $\tilde{X}_2 = P$. This approach provides an efficient way to calculate the minimum variance and determine the squeezed properties of the magnon state in terms of quadrature fluctuations.

## V. ADDITIONAL DATA

### A. Magnon displacement amplitude calibration

In the experiment, displacement operations $D(\alpha)$ are implemented via microwave pulses. For a fixed-duration microwave pulse, the amplitude of the displacement value $|\alpha|$ is determined by the amplitude of the microwave pulse, which needs to be calibrated by determining the ratio between $|\alpha|$ and the microwave-drive amplitude (i.e., the scale factor between them). This is performed by preparing the Kittel mode in coherent states with different displacement values $|\alpha|$, generated by applying microwave pulses with different amplitudes to the vacuum state of magnons. Also, the qubit is prepared in the ground state. Then, we employ the magnon-assisted Raman process to have the qubit resonantly interact with the Kittel mode for a varying time $t$. This yields a swapping curve for each occupied Fock state $|n\rangle$ of magnons. For a given displacement value $\alpha$, the obtained swapping curve is fitted to $P_{|f\rangle}(t) = \frac{1}{2}[1 - \sum_n \tilde{\rho}_{nn} \cos(2\sqrt{n} g_0 t)]$, where $P_{|f\rangle}(t)$ is the occupation probability of the qubit in the second-excited state $|f\rangle$. The mean magnon number is calculated using $\bar{n} = |\alpha|^2 = \sum_n n\tilde{\rho}_{nn}$ and hence $|\alpha|$ is obtained.

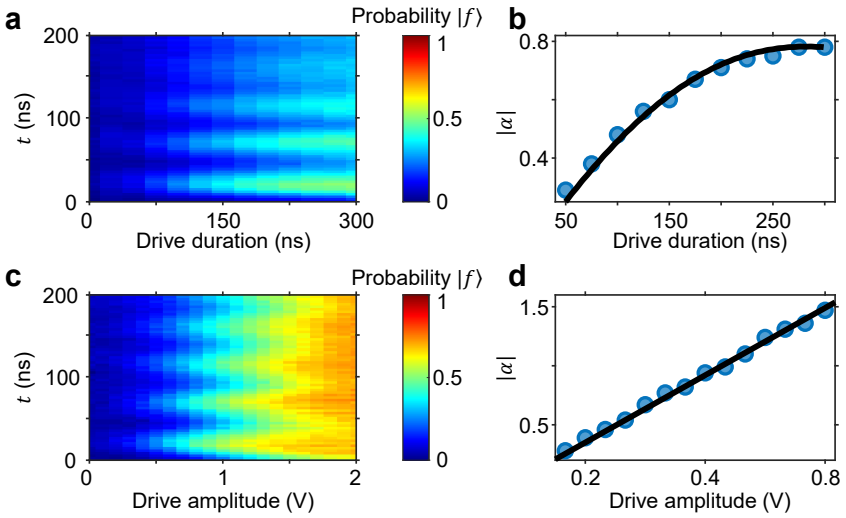


FIG. S2. **Magnon displacement amplitude calibration. a,** Experimental results showcasing the calibration of the drive amplitude for the first microwave pulse applied to the magnon mode. The output voltage corresponds to the drive amplitude and is fixed at 0.2 V. The horizontal axis represents the microwave drive duration, and the vertical axis illustrates the resonant swap interaction time between the qubit and the magnon mode. **b,** Fits (blue circles) to the qubit-magnon swap curves in **a**. The black solid curve denotes the numerical result, which gives the drive amplitude 11.7 MHz. **c,** Experimental results showcasing the calibration of the drive amplitude for the second microwave pulse applied to the magnon mode (i.e., the pulse for magnon displacement). The pulse duration is 35 ns. The horizontal axis represents the microwave drive amplitude, and the vertical axis illustrates the resonant swap interaction time. **d,** Fits (blue circles) to the qubit-magnon swap curves in **c**. The black solid line gives a linear fit $|\alpha| = 0.95A + 0.16$, where $A$ represents the drive amplitude. The maximum occupation number in the magnon Fock states is truncated at $n = 9$.

There are two microwave pulses for driving the Kittel mode in the experimental sequence of operations (see Fig. 1b in the main text). The first microwave pulse has a varying duration ranging from 0 to 250 ns, while the second microwave pulse has a fixed time duration at 35 ns. Ideally, if the duration of the microwave pulse is much shorter than the magnon lifetime ($T_{1,m} = 145$ ns), the displacement amplitude is proportional to both the amplitude and duration of the microwave pulse. However, the duration of the first pulse could be comparable to the magnon lifetime, resulting in a driven dissipative dynamics. Therefore, calibration should be performed separately for these two pulses. The calibration for the first microwave pulse is shown in Fig. S2a, where the qubit-magnon swapping curves with different microwave pulse durations and a fixed output voltage of 0.2 V are shown. The corresponding numerical fitting is shown in Fig. S2b, from which we obtain the Rabi frequency of the first drive at $\Omega_{m,d} = 11.7$ MHz. Here, $|\alpha|$ exhibits a nonlinear dependence on the drive duration as a result of the magnon decay. The amplitude calibration for the second microwave pulse (i.e., the magnon displacement operation) is shown in Fig. S2c, where the swapping curves with different microwave pulse amplitudes are shown. Because the pulse duration is fixed and reasonably short, the ratio of the displacement value to the microwave drive amplitude is linear. The scale factor is fitted by linear regression. This linear fitting is shown as the solid line in Fig. S2d, with the scale factor $c = |\alpha|/A \approx 0.95$.

### B. Qubit spectroscopy under the Autler-Townes drive

We performed qubit spectroscopy under the Autler-Townes (AT) drive to determine the tunable qubit frequency. A strong drive resonant with $\omega_{ef}$ is applied, generating an AT splitting. Simultaneously, a relatively weak probe was used to measure the qubit's eigenfrequencies under the AT drive. As expected, the qubit's eigenfrequencies split into two branches due to the AT effect, corresponding to the transitions from $|g\rangle$ to the dressed states $|+\rangle$ (upper branch) and $|-\rangle$ (lower branch), respectively.

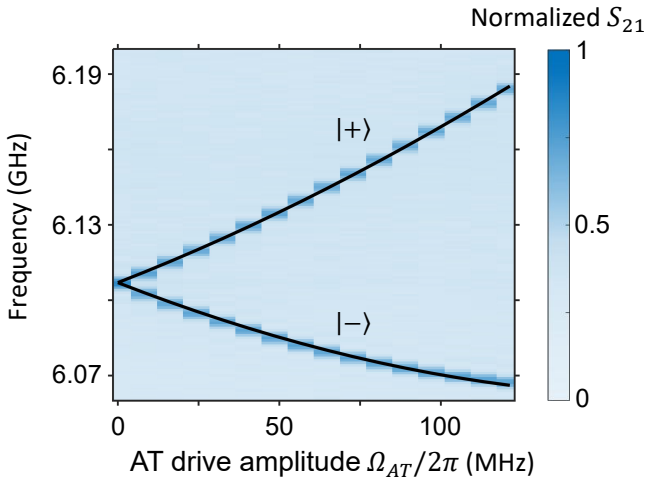


FIG. S3. **Autler-Townes splitting of the qubit.** Qubit spectroscopy is performed versus the AT drive amplitude $\Omega_{\rm AT}$. The black solid curves are numerical fits. The upper (lower) branch corresponds to the transition from $|g\rangle$ to the dressed state $|+\rangle$ ($|-\rangle$). The frequency of the upper branch is defined as the transition frequency $\omega_q$ of the tunable qubit.

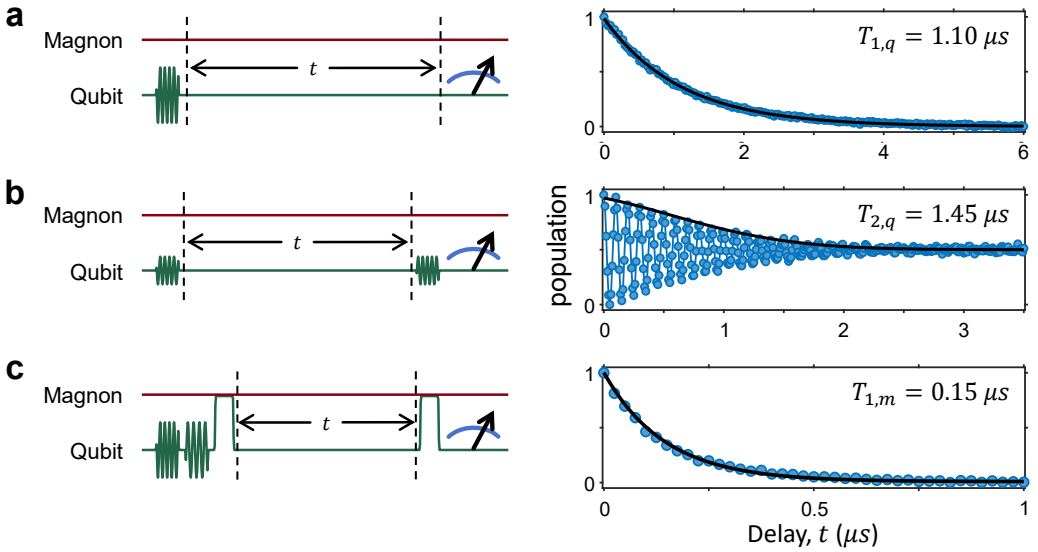


FIG. S4. **Quantum coherence measurement. a,** Left: Sequence of operations for measuring the qubit lifetime $T_{1,q}$. Right: Experimental data for the qubit lifetime $T_{1,q}$. The experimentally measured qubit population in $|e\rangle$ (blue dots) is fit with an exponential decay (solid curve) and the fitting gives a qubit lifetime $T_{1,q} = 1.10$ $\mu$s. **b,** Left: Sequence of operations for measuring the qubit pure dephasing time $T_\phi$. Right: Experimental data for the qubit pure dephasing time $T_\phi$. Blue dots are experimentally measured probabilities of the qubit in $|e\rangle$, and the black solid curve is fitted to the envelope of oscillations, giving a qubit pure dephasing time $T_\phi = 1.45$ $\mu$s. **c,** Left: Sequence of operations for measuring the magnon lifetime $T_{1,m}$. Right: Experimental data for the magnon lifetime $T_{1,m}$. The probability of the magnon in $|1\rangle$ is inferred from the probability of the qubit in $|f\rangle$ (blue dots) via the magnon-assisted Raman process. The data are fitted with an exponential decay (solid curve), giving a magnon lifetime $T_{1,m} = 145$ ns.

### C. Coherence measurement

Time-domain measurements on the transmon qubit are performed to extract information about the quantum coherence of the system. Specifically, we measure the qubit lifetime ($T_{1,q}$), qubit pure dephasing time ($T_\phi$) and magnon lifetime ($T_{1,m}$). The qubit lifetime $T_{1,q}$ is measured by first preparing the qubit in the first-exciteed state $|e\rangle$ and then measure the population in $|e\rangle$ ($P_e$) after a varying delayed time $t$, while the qubit pure dephasing time $T_\phi$

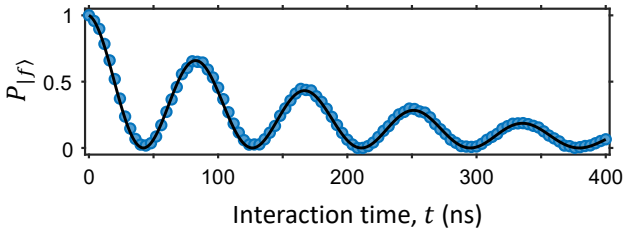


FIG. S5. **Qubit-magnon resonant swap.** Blue dots illustrate the experimentally obtained qubit-magnon swapping, and the black solid curve is the numerical fit by using a cosine function with an exponential decay. The numerical fitting extracts the coupling strength $g_0/2\pi = 6.0$ MHz for the state swap between $|f,0\rangle$ and $|g,1\rangle$.

is determined via Ramsey interference measurements.

To measure the magnon lifetime $T_{1,m}$, the system is first prepared in the state $|f,0\rangle$ using two consecutive $\pi$-pulses for the $|g\rangle \rightarrow |e\rangle$ and $|e\rangle \rightarrow |f\rangle$ transitions. By utilizing the magnon-assisted Raman process, the population in $|f\rangle$ is fully swapped into the magnon mode by properly choosing the swapping time $t_{\rm swap} = \frac{\pi}{2g_0}$, resulting in the system state $|g,1\rangle$. After a varying time $t$, the remaining magnon population is swapped back to the qubit for measurement.

By fitting the experimental data, we obtain the qubit lifetime $T_{1,q} = 1.10$ $\mu$s, qubit pure dephasing time $T_\phi = 1.45$ $\mu$s and magnon lifetime $T_{1,m} = 145$ ns, respectively, from which we calculate the cooperativity $C$ of the system and determine the magnon decay rate used in the numerical simulations.

### D. Qubit-magnon resonant swap via the magnon-assisted Raman process

The resonant swap between $|f,0\rangle$ and $|g,1\rangle$ is essential in our experiment. By fitting the swapping curve, we obtain the microwave-induced coupling strength $g_0$. The system is first prepared in the state $|f,0\rangle$ via two $\pi$-pulses for the $|g\rangle \rightarrow |e\rangle$ and $|e\rangle \rightarrow |f\rangle$ transitions. Subsequently, a microwave drive with amplitude $\Omega/2\pi = 58$ MHz at the frequency $\omega_d = 2\omega_{ge} + \eta - \omega_m$ is applied for initiating the magnon-assisted Raman process. After a duration $t$ elapses, we measure the probability of the qubit in $|f\rangle$, i.e., $P_{|f\rangle}$, which is a sinusoidal curve with an exponential decay envelope. The numerical fit (solid curve) gives a coupling strength of $g_0/2\pi = 6.0$ MHz, which agrees well with the result given by the Fourier transformation (Fig. 1c in the main text).


[1] D. Xu, X.-K. Gu, H.-K. Li, Y.-C. Weng, Y.-P. Wang, J. Li, H. Wang, S.-Y. Zhu, and J. Q. You, Quantum control of a single magnon in a macroscopic spin system, Phys. Rev. Lett. **130**, 193603 (2023).

[2] D. Xu, X.-K. Gu, Y.-C. Weng, H.-K. Li, Y.-P. Wang, S.-Y. Zhu and J. Q. You, Macroscopic Bell state between a millimeter-sized spin system and a superconducting qubit, Quantum Sci. Technol. **9**, 035002 (2024).

[3] S. Autler and C. Townes, Stark effect in rapidly varying fields, Phys. Rev. **100**, 703 (1955).

[4] A. Imamoğlu, Cavity QED Based on Collective Magnetic Dipole Coupling: Spin Ensembles as Hybrid Two-Level Systems, Phys. Rev. Lett. **102**, 083602 (2009).

[5] M. Boissonneault, J. M. Gambetta, and A. Blais, Dispersive regime of circuit QED: Photon-dependent qubit dephasing and relaxation rates, Phys. Rev. A **79**, 013819 (2009).

[6] M. Pechal, L. Huthmacher, C. Eichler, S. Zeytinoğlu, A. A. Abdumalikov, S. Berger, A. Wallraff, and S. Filipp, Microwave-Controlled Generation of Shaped Single Photons in Circuit Quantum Electrodynamics, Phys. Rev. X **4**, 041010 (2014).

[7] Y. Tabuchi, S. Ishino, A. Noguchi, T. Ishikawa, R. Yamazaki, K. Usami, and Y. Nakamura, Coherent coupling between a ferromagnetic magnon and a superconducting qubit, Science **349**, 405 (2015).

[8] J. Johansson, P. Nation, and F. Nori, QuTiP 2: A python framework for the dynamics of open quantum systems, Computer Physics Communications **184**, 1234-1240 (2013).